Molecular-dynamics simulation of crystalline *trans*-polyacetylene

P. Papanek and J. E. Fischer
Materials Science and Engineering Department and Laboratory for Research on the Structure of Matter, University of Pennsylvania, Philadelphia, Pennsylvania 19104-6272
(Received 1 July 1993)

Constant-pressure molecular-dynamics simulations of rigid, infinitely long polyacetylene chains were performed for various temperatures and pressures. The experimentally observed anisotropic lattice thermal expansion and compressibility were qualitatively well reproduced by the simulations. The model lattice exhibits considerable jump diffusion along chain axes already at room temperature, with the onset of liquidlike diffusion above 400 K accompanied by orientational disorder of chain projections in the *ab* plane. The polarized vibrational density of states for $E \leq 25$ meV is in good agreement with $G(E)$ spectra derived from inelastic incoherent neutron-scattering experiments. By analyzing different contributions to chain motions, peaks in $G(E)$ at 3.5, ~ 8, and ~ 20 meV can be assigned to rigid-chain vibrations along the chain axis, vibrations in the *ab* plane, and chain librations, respectively.

I. INTRODUCTION

Polyacetylene $(CH)_x$ is the simplest conjugated polymer. The chain backbone is formed by alternating single and double bonds. It can be prepared by catalytic polymerization of acetylene gas; the first synthesized polyacetylene was a grey powdery material insoluable in common solvents and did not possess any exciting properties. By changing the reaction conditions Shirakawa and co-workers[1,2] were successful in preparing free-standing films with metallic luster. The dramatic growth of interest in this polymer began after 1978 when Chiang *et al.*[3] announced that the electrical conductivity of such films can be increased by as much as 13 orders of magnitude upon doping with various electron-accepting and electron-donating species. The interesting physical properties of $(CH)_x$ have been well described within the framework of a model proposed by Su, Schrieffer, and Heeger (SSH),[4] in which the low energy excitations are solitons, polarons, and bipolarons.

The degree of crystallinity of freshly synthesized $(CH)_x$ films can reach almost 90%. Low-temperature polymerization produces predominantly the *cis* configuration, but upon heat treatment or heavy doping a *cis*-to-*trans* isomerization occurs. Modifications in the preparation method led to further improvement of the sample quality. The methods devised by Naarmann and Theophilou,[5] Akagi *et al.*,[6] and Cao *et al.*[7] yield high-density (~ 1 g/cm^3) $(CH)_x$ films which can be stretch oriented to achieve a mosaic distribution of less than 10° [full width at half maximum (FWHM)]. This was extremely important for the ongoing research on the structure of $(CH)_x$.

The crystal structures of both *trans*- and *cis*-polyacetylene have been exhaustively investigated by various diffraction techniques. The structure of *cis*-$(CH)_x$ was found to be orthorhombic[8] with space group *Pnam*; *trans*-$(CH)_x$ has a monoclinic structure[9,10] (with the monoclinic angle $\beta = 92°$) and the space group was identified as either $P2_1/n$ or $P2_1/a$. The difference between these two is that the single and double bond sequences in the two nearest (inequivalent) neighbor chains are in phase for $P2_1/a$ and out of phase for $P2_1/n$ (Fig. 1). Recent x-ray-diffraction studies[11] based on the analysis of individual off-axis peak intensities confirm that the correct space group is $P2_1/n$.

From the structural point of view, doped $(CH)_x$ derivatives represent anisotropic guest–host systems with competing interactions, exhibiting strong bonding in one direction (along the polymer chains) and weak bonding in two directions (interchain interactions). The herringbone interchain configuration of pristine *trans*-$(CH)_x$ transforms upon doping to a triangular or square arrangement, with planar symmetry motifs depending on dopant size.[12] These structural changes are well correlated with

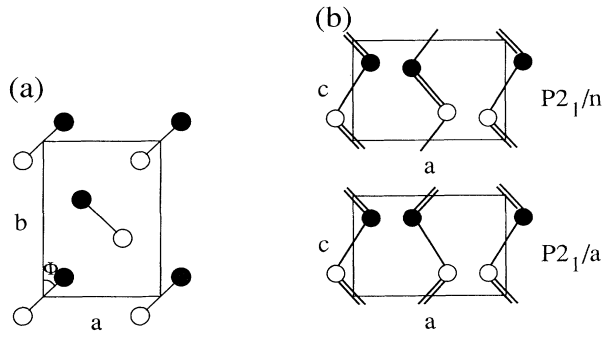

FIG. 1. Schematic structures of *trans*-polyacetylene. Each circle represents a (CH) group; alternating groups on each chain are depicted as open and solid circles to emphasize the dimerization. (a) *ab* plane, with setting angle Φ defined as the angle between the plane of the chain and the *b* axis; (b) out-of-phase and in-phase structures as described by space groups $P2_1/n$ and $P2_1/a$ respectively.

changes in transport and electronic properties. The evolution of these structures is determined by successive activation of chain rotations and translations; thus in order to understand the intercalation processes it is of great importance to have deeper knowledge of the lattice dynamics. Also, although the SSH model is in principle one-dimensional, it has been recognized that the three-dimensional (3D) periodic arrangement of the polymer chains plays a role in the interchain hopping,[13] and the effect of chain dynamics on the interchain hopping is still not very clear. The importance of interchain interactions for improving the conductivity of alkali-metal-doped oriented polyacetylene has been convincingly demonstrated by recent high-pressure experiments.[14]

The interchain packing of *trans*-$(CH)_x$ exhibits unusual temperature dependence. Ma *et al.*[15] carried out x-ray experiments which showed that the a parameter expands twice as fast as b, accompanied by a 6° increase of the setting angle Φ with increasing T. The b/a ratio decreased from 1.83 to 1.79 as T increased from 129 K to 513 K, consistent with the tendency to form a triangular lattice ($b/a = \sqrt{3}$). A similarly high anisotropy was found in interchain compressibilities[16] ($\Delta a/a = 8.3 \times 10^{-3}\text{kbar}^{-1}$, $\Delta b/b = 3.8 \times 10^{-3}$ kbar^{-1} below 6 kbar), with lattice stiffening above 6 kbar as close packing is approached. For comparison, polyethylene $(CH_2)_x$, which has a similar molecular structure and also crystallizes in the herringbone arrangements of chain projections[17] (orthorhombic space group *Pnma*, $a = 7.15$ Å, $b = 4.91$ Å, $c = 2.55$ Å), exhibits similar anisotropic behavior, but in the opposite way[18]—the long axis expands faster than the short one, and the setting angle decreases with T. This difference between $(CH)_x$ and $(CH_2)_x$ was explained as the result of the tendency of both lattices to approach triangular chain packing with increasing temperature.[15]

Until recently, experimental information on the lattice dynamics in polyacetylene was limited to infrared and Raman $Q = 0$ intrachain modes. The advent of highly oriented films has made it possible to obtain polarization and energy information on general lattice modes by using incoherent inelastic neutron scattering.[19] Using two scattering geometries and summing over different scattering angles, hydrogen motions parallel and perpendicular to the average chain axis can be separately detected, and from the scattering spectra the polarized density of vibrational states $G(E)$ can be evaluated. Due to the inherent anisotropy of $(CH)_x$, pronounced differences between $G_\parallel$ and $G_\perp$ were found, especially in the low-frequency region, both for *cis* and *trans* isomers. One of the main motivations for the present work was to supply complementary information on the lattice vibrations, thus enabling unambiguous identification of distinct peaks in the measured $G(E)$.

II. SIMULATION METHODS

We performed constant-pressure molecular-dynamics (MD) simulations for a range of temperatures and pressures using a method similar to the one developed for solid n-alkanes.[20] The simulation box consisted of a 5×3 array of cells produced by eight crystallographic units [as in Fig. 1(a)] placed on top of each other; i.e., each cell contained two polymer chains with 16 (CH) groups. The geometry corresponding to the space group $P2_1/n$ was used in all simulations. Because of the low flexibility of the alternating double bonds, we have made the assumption of complete rigidity and planarity of the polymer chains. This prevents us from obtaining any information about intrachain vibrations (which occur mainly at high frequencies). The resulting simplification enables us to perform several simulation runs for very long times, which is important for the correct determination of the interchain motion. Another approximation was made by setting the angle $\beta = 90°$; i.e., the chains were assumed perpendicular to the ab plane.

Periodic boundary conditions were imposed in all three directions; in the c direction (parallel to chain axes) this together with the proper constant box length $L_c = 8c$ (where $c = 2.457$ Å is the crystallographic lattice constant determined by Zhu *et al.*[11]) mimicked the "infinity" of simulated chains. The following chain geometry was used in the calculations:[10,21] C—C bond length 1.46 Å, C=C bond length 1.35 Å, C—H bond length 1.08 Å, C—C—H angle 117°, and C–C=C angle 122° [this value being in accord with the measured value of the c parameter; modified neglect of differential overlap (MNDO) calculations predict the value 124.9°].

Intermolecular interaction energies were computed using the semiempirical atom-atom pair potential function

$$V(d) = Ad^{-6} + B \exp(-Cd), \tag{1}$$

where d is the distance between two atoms in different molecules and the values of constants A, B, and C for C $\cdots$ C, C $\cdots$ H, and H $\cdots$ H interactions were adopted from parameter set VII of Table II of Williams.[22] We should stress that this requires placing the hydrogen repulsion and attraction centers 1.04 Å away from carbon. We adopted this potential function instead of the more frequently used Lennard-Jones potential because the latter is rather soft when used in high-pressure simulations. To avoid unphysical interactions of a particle with its images in neighboring simulation boxes, the potentials were truncated at a cutoff distance 8.5 Å for C $\cdots$ C interactions, and 6 Å for C $\cdots$ H and H $\cdots$ H interactions.

In order to follow T-dependent changes of the interchain distances, the dimensions of the simulation box must be introduced into the Lagrangian of the system as additional time-dependent generalized coordinates. It was shown by Andersen[23] that the phase trajectories generated by the new Lagrangian of the "extended" system yield time averages of physical (thermodynamic) properties that reproduce quite well the ensemble averages of the original system for an isoenthalpic–isobaric (NPH) ensemble. This method was generalized by Parrinello and Rahman[24] who proposed a scheme that allows the volume *and* the shape of the periodic cell to vary with time.

If we denote the vectors along the sides of the simulation box as $\mathbf{L}_a = (a_1, a_2, 0)$, $\mathbf{L}_b = (b_1, b_2, 0)$, and

$\mathbf{L}_c = (0, 0, c_3)$, where the a's and b's are additional time-dependent variables of the system, then the position vector of the ith atom in the αth molecule can be expressed as

$$\mathbf{r}_{\alpha i} = s_{1\alpha}\mathbf{L}_a + s_{2\alpha}\mathbf{L}_b + s_{3\alpha}\mathbf{L}_c + \tilde{\mathbf{r}}_{\alpha i} \ , \qquad (2)$$

where $0 \leq s_{j\alpha} \leq 1$, $(j = 1, 2, 3)$ are the scaled frame coordinates of the center of mass of the αth molecule and $\tilde{\boldsymbol{r}}_{\alpha i}$ is the relative position of the ith atom in the αth molecule with respect to the center of mass of that molecule. The coordinates of $\tilde{\mathbf{r}}_{\alpha i}$ can be easily determined from the geometry and orientation of the chain projection. Then the Rahman-Parrinello Lagrangian for our model can be written as

$$\begin{aligned}\mathcal{L} = \frac{1}{2}M \sum_{\alpha} & (\dot{s}_{1\alpha}a_1 + \dot{s}_{2\alpha}b_1)^2 \\ & + (\dot{s}_{1\alpha}a_2 + \dot{s}_{2\alpha}b_2)^2 + (\dot{s}_{3\alpha}c_3)^2] + \frac{1}{2}I \sum_{\alpha} \dot{\varphi}_{\alpha}^2 \\ & + \frac{1}{2}W(\dot{a}_1^2 + \dot{b}_1^2 + \dot{a}_2^2 + \dot{b}_2^2) \\ & - \sum_{\alpha} \sum_{\beta > \alpha} \sum_{i,j} V_{ij}(|\mathbf{r}_{\alpha i} - \mathbf{r}_{\beta j}|) - P_{\text{ext}}\Omega \ , \qquad (3)\end{aligned}$$

where M is the mass of the chain, I its tensor of inertia, φ_α is the angle between the chain projection of the αth molecule onto the ab plane and the x axis of the reference coordinate system, P_{ext} is the imposed external pressure, and $\Omega = \mathbf{L}_a \cdot \mathbf{L}_b \times \mathbf{L}_c$ is the time-dependent volume of the simulation box. The adjustable parameter W corresponds to the mass of a virtual piston compressing the simulation box. A low value of W would result in fast oscillations of the size and shape of the box, and a large value would lead to slow exploration of the phase space (a deeper discussion of this parameter is given by Andersen[23] and by Nosé and Klein[25]). In our simulations it was set equal $5M$.

The Lagrangian equations of motion form a system of 124 coupled second-order differential equations. Since the well-known Verlet algorithm usually used in standard MD simulations is not applicable for extended systems without considerable modifications, other numerical methods to solve the differential equations had to be used instead. Both fourth-order Adams-Moulton[26] and fifth-order Gear[27] predictor-corrector methods were applied to solve the system with almost identical results. Because of the high precision of such multistep methods (and the assumed chain rigidity), the time step can be relatively long; we used a 4 fs (fs $= 10^{-15}$ s) time step in all simulation runs, and the total time of some simulations was more than 60 ps (i.e., 15 000 timesteps).

Several runs have been done for $P_{\text{ext}} = 1$ atm at various temperatures in the interval $170\,\text{K} \leq T \leq 420\,\text{K}$. A desired equilibrium T was achieved by assigning initial chain velocities which satisfy the Boltzmann distribution for that T and by an occasional rescaling of velocities during equilibration runs. The equilibration periods lasted at least 2000 time steps, during which the evolution of the system was carefully examined. In all simulations good equipartitioning of the thermal energy (resulting in comparable translational and rotational temperatures) was achieved. One advantage of the imposed rigidity of the chains is the fact that there is no necessity to equilibrate the inter- and intramolecular temperatures or to employ explicit temperature control (e.g., by means of massive stochastic collisions) in order to achieve such equilibrium, since that could modify the long-time (low-frequency) dynamics of the system.

After equilibration a "production" run for a total time varying from 20 to 60 ps has followed, during which the trajectories have been recorded. From these data the thermodynamic and structural averages were calculated. The same procedure was repeated for pressures 1, 3, 5, and 6 kbar and $T \approx 250$ K. The computations were performed on Stardent 3000, Silicon Graphics IP7, and Solbourne 5/500 computers, and the net computation time for a 40 ps run was approximately 200 CPU hours.

III. AVERAGE STRUCTURE vs TEMPERATURE

A brief summary of the simulation results for atmospheric pressure and different temperatures is presented in Table I. The calculated T-dependent relative changes of lattice parameters a and b confirm the experimentally observed anisotropy, with the shorter side a expanding much faster than b (Fig. 2). The measured linear expansion coefficients determined from the initial slopes of $\Delta a/a$ and $\Delta b/b$ were 9.0×10^{-5} K^{-1} for a and 4.5×10^{-5} K^{-1} for b (this value being quite similar to the c–axis expansion of graphite), while least-squares fits of the slopes of calculated $\Delta a/a$ and $\Delta b/b$ give 7.7×10^{-5} K^{-1} and 3×10^{-5} K^{-1} respectively. Also,

TABLE I. Temperature-dependent structural parameters of crystalline *trans*-polyacetylene calculated from the MD simulation at pressure $P = 1$ atm.

T imposed (K)	equilibrium T (K)	run time (ps)	a (Å)	b (Å)	Φ (deg)	γ (deg)
150	173	60	3.838	7.648	40.69	90.02
200	205	20	3.847	7.649	41.02	89.97
250	249	40	3.853	7.659	41.24	90.03
300	308	40	3.876	7.664	41.49	89.95
350	351	30	3.885	7.696	41.70	89.87
375	378	60	3.904	7.688	41.73	89.89
400	404	40	3.909	7.711	41.04	89.94
425	417	30	4.105	7.456	40.44	94.29

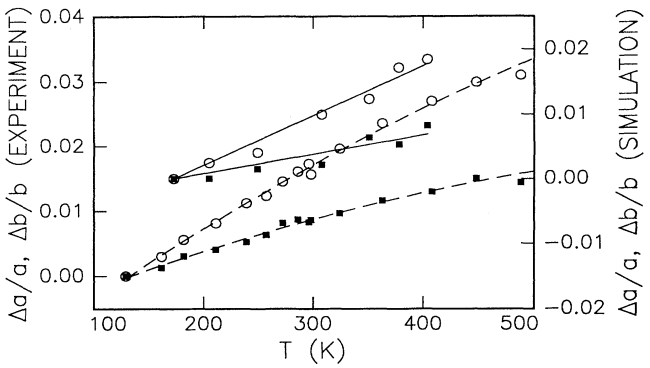

FIG. 2. Anisotropic thermal expansion in the ab plane (circles, $\Delta a/a$; squares, $\Delta b/b$). Solid curves derived from MD simulations (right scale); dashed curves are the x-ray results (Ref. 15) (left scale). All curves are guides to the eye. Note that the scales are the same but the origins have been shifted for clarity.

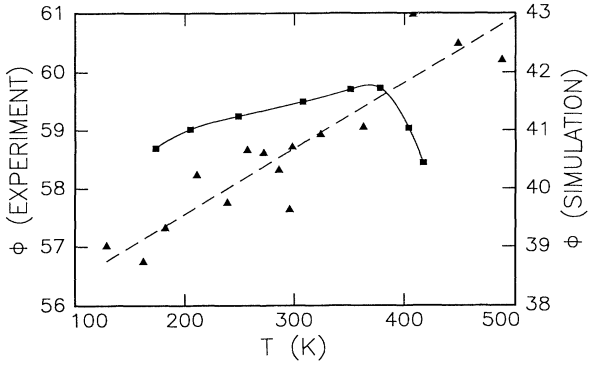

FIG. 3. Temperature dependence of the setting angle Φ (deg). Solid curve and squares derived from MD simulations (right scale); dashed curve and triangles are the x-ray results (Ref. 15) (left scale). Both curves are guides to the eye. Note that the scales are the same but the origins have been shifted for clarity.

the 300 K x-ray data gave $a = 4.095$ Å, $b = 7.386$ Å, and $\Phi = 55°$, whereas the simulation results are smaller for a and greater for b ($a = 3.876$ Å, $b = 7.664$ Å) and $\Phi = 41.5°$. Thus the anisotropy in both the lattice constants and the expansion coefficients are more pronounced in the model as compared to experiment.

Normally, thermal expansion driven by lattice anharmonicity results in expansion coefficients which diverge as T approaches the melting point. The measured data, however, exhibit a slightly negative curvature of both $\Delta a/a$ and $\Delta b/b$, suggesting a continuous approach to a new high-T phase with a definite b/a ratio. The simulation results for temperatures up to 400 K do not show such curvature and are in fact too scattered to suggest anything but linear behavior.

The T dependence of b/a is also correctly reproduced. With increasing T, b/a decreases linearly, confirming the tendency towards a close packed triangular lattice with limiting value $b/a = \sqrt{3}$. The static mass density of a polyacetylene chain projected onto the ab plane is more elliptical than disklike, but if chain rotations were unrestricted, the dynamic average would be circular and the 2D lattice (in ab plane) should become isotropic. The experiments as well as the simulation confirm that the chain rotations are indeed hindered and the rotational and translational motions in the ab plane are coupled, so that the anisotropy is conserved in the whole temperature region.

The faster expansion of a than b forces an increase in the setting angle Φ, as shown in Fig. 3. Here we see bigger differences between the observed and calculated values. Surprisingly, the simulated system also exhibits a fast drop of Φ above 400 K. This is accompanied by an abrupt decrease of the b/a ratio to the value 1.82 at 417 K. All this suggests a phase transition in the simulated system. A visual examination of the motion revealed an onset of disorder in the orientation of setting angles and longitudinal diffusion of the chains along the c direction. This raises the interesting question whether the longitudinal diffusion is directly influenced by rotational defects and vice versa. To find an answer, we analyzed the rotational and longitudinal motions of the chains in more detail.

First the distributions of setting angles and center of mass displacements in the c direction from a mean lattice position have been calculated. Note that a chain jump of a distance c with respect to other chains gives a configuration equivalent to the initial one; therefore the mean lattice point in the c direction must be calculated by some other method than by simply averaging the c coordinates of the chain centers of mass Z_M^α. We adopted the method described by Ryckaert and Klein[20] in which the lattice point Z_0 is defined at each time step by requiring that the quantity

$$X = \sum_\alpha \cos 2\pi (Z_M^\alpha - Z_0)/c \ , \tag{4}$$

where the summation is carried out over all chains in the box, is maximum. This defines the mean lattice position only to within an integer number of cell lengths c; thus the displacement of a particular chain α as a function of time is then properly defined as

$$\Delta Z_M^\alpha(t) = [Z_M^\alpha(t) - Z_0(t)] - c \ \text{round} \{[Z_M^\alpha(t) - Z_0(t)]/c\} \ , \tag{5}$$

where round(x) represents the closest integer to x.

The distributions of setting angles and displacements calculated from the trajectories of all chains are shown in Fig. 4. At the lowest temperature [Fig. 4(a) for $T = 173$ K] the setting angles are sharply distributed about the average values ($\pm 40.7°$ because of the two inequivalent chains in the unit cell) with maximum deviations approximately $\pm 20°$. The displacements of chains in the c direction are at this temperature also well distributed about the mean lattice position, the maximum oscillation being roughly ± 0.5 Å. At higher T, the distribution of Φ did not change very much, but the distribution of displacements broadened significantly. At 417 K the displace-

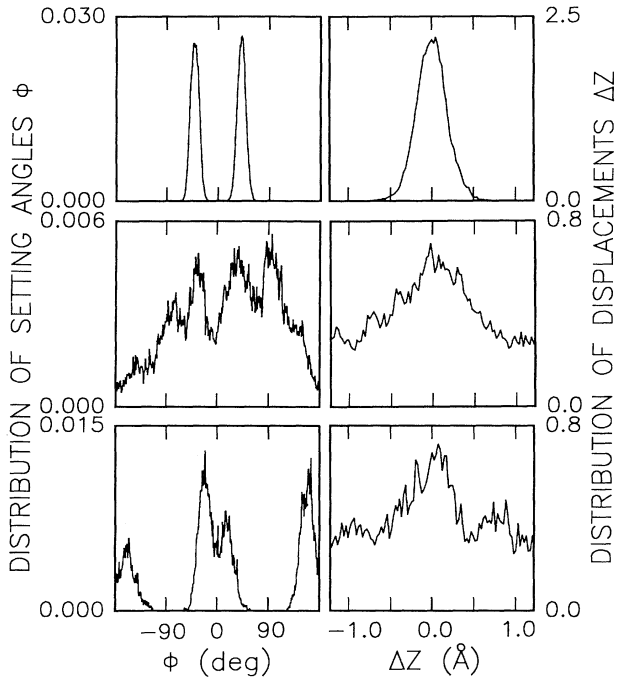

FIG. 4. Distributions of setting angles Φ and displacements in the c direction, Δz. Top row, 173 K; middle row, 417 K (first half of simulation run); bottom row, 417 K (second half of simulation run).

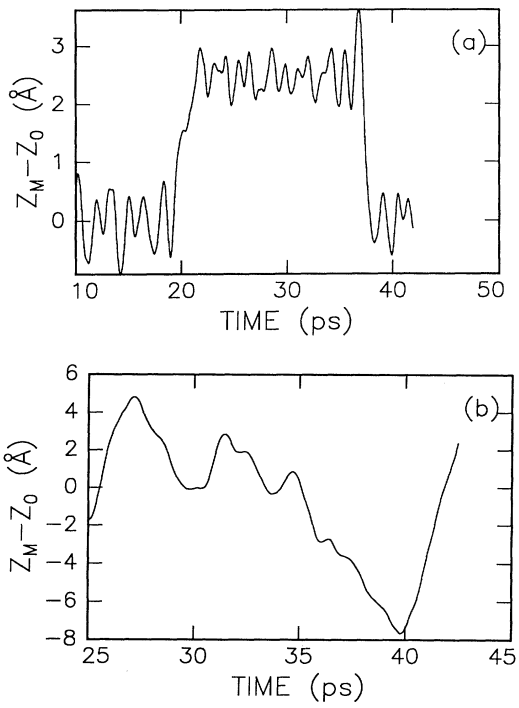

FIG. 5. Motion of a typical chain along c with respect to a reference lattice point: (a) 308 K, showing jump diffusion, and (b) 404 K, showing more liquidlike diffusion.

ment distribution over the first half of the run is already very broad (suggesting that the concept of an average lattice in the c direction loses its meaning), and the setting angles are clearly disordered [Fig. 4(b)]. This disorder could however correspond to a transition period, since in the second half of the simulation a significant fraction of chains adopt parallel and antiparallel orientations (±20°) with respect to b [Fig. 4(c)]. Such oscillatory behavior is typical for first-order phase transformations simulated in small systems; due to the small size, the energetically costly interface between the two phases cannot be created. Since the simulated transition has not been seen experimentally, we did not examine this point in further detail. Interestingly, the simulated order-disorder transition is quite close to the extrapolated 414 K melting temperature of n-alkanes with infinite chain length.[28]

The broadening of the distribution of displacements along chain axes, noticeable already at 308 K, is the result of jump diffusion along the c direction. Two such jumps of a particular chain with respect to the mean lattice position are shown in Fig. 5(a). The average jump frequency at this temperature was 1 jump every 20 ps. Naturally, the jump frequency increases with temperature, and above 400 K a smooth transition to a liquidlike diffusion in the c direction occurs [Fig. 5(b)]. Whereas the jump diffusion does not introduce any rotational defects, the onset of the liquidlike diffusion is accompanied by orientational disorder with a possible transition to a high-T phase with parallel and antiparallel orientations of chain projections.

IV. AVERAGE STRUCTURE vs PRESSURE

The behavior of *trans*-$(CH)_x$ under elevated pressure has also been investigated. The results are summarized in Table II and Fig. 6. Both a and b decrease significantly with increasing P, but the lattice stiffens in the a direction already at 1 kbar, while b decreases approximately linearly with pressure up to 5 kbar at which a noticeable stiffening occurs. The initial linear compressibility of a calculated from the first two simulation points is 8.3×10^{-3} kbar^{-1}, as is the experimentally measured value. Above 1 kbar a least-squares linear fit yields an average value 3.4×10^{-3} kbar^{-1}. The simulated compressibility in the b direction in the range from 0 to 5 kbar is 5×10^{-3} kbar^{-1}, higher than the experimentally found 3.8×10^{-3} kbar^{-1}, and above 5 kbar it drops to 1×10^{-3} kbar^{-1}.

The initial anisotropy at lower pressures is consistent with the anisotropic temperature behavior. In the interval from 1 to 5 kbar the simulated lattice displays an "inverse" anisotropy, with the compressibility in the b direction greater than in the a direction. In this range also an increase in the setting angle of about 1° was observed. The b axis stiffens significantly at 5 kbar, which is close to the experimentally observed value of 6 kbar. The slight difference can be partially due to the rigidity of the simulated chains.

The average value of the angle γ between the a and b axes stayed very close to 90° during all simulations in the entire P range. This is contrary to the conclusion from

TABLE II. Calculated changes of lattice parameters with hydrostatic pressure.

P_{ext} (kbar)	equilibrium T (K)	run time (ps)	a (Å)	b (Å)	Φ (deg)	γ (deg)
0.001	249	40	3.853	7.659	41.24	90.03
1.0	242	40	3.821	7.613	40.94	89.98
3.0	243	40	3.789	7.539	41.23	89.98
5.0	259	40	3.771	7.467	41.96	90.02
6.0	269	40	3.753	7.459	41.17	90.01

the x-ray study[16] that a transformation from centered rectangular ($\gamma = 90°$) at $P = 0$ to oblique ($\gamma = 91° - 92°$) at high pressure occurs with a threshold below 0.5 kbar. This discrepancy could indicate that in order to correctly simulate the evolution of γ with P, the correct monoclinic structure with $\beta = 92°$ must be modeled. A definite conclusion of this problem will require more precise experiments with higher resolution in P and Q as well as more detailed simulations.

V. LATTICE DYNAMICS

Dynamic trajectories obtained from the simulations described above were stored and used later to obtain information about the dynamics of the lattice modes in *trans*-$(CH)_x$. Inelastic neutron-scattering experiments on *cis*-$(CH)_x$ reveal considerable anisotropy in the vibrational densities of states polarized parallel and perpendicular to c.[19] Similar data for *trans*-$(CH)_x$, of somewhat lesser quality, is now available and is shown in Fig. 7. Although the features are not well resolved, differences between $G_{\|}$ and $G_{\perp}$ are clearly apparent.

A harmonic approximation of the density of vibrational states can be computed as the temporal Fourier transform of the velocity autocorrelation function.[27] Thus, except for a proper normalization constant, $G(\omega)$ can be expressed as

$$G(\omega) = \frac{1}{N} \sum_{\alpha} \int_{-\infty}^{\infty} \langle \mathbf{v}_{\alpha}(t) \mathbf{v}_{\alpha}(0) \rangle \, e^{-i\omega t} dt \ , \qquad (6)$$

where $\mathbf{v}_{\alpha}$ is the velocity of the αth particle, N is the total number of particles, and the brackets denote ensemble averaging. In order to simulate the neutron-scattering results the contributions of different particles to the density of states must be weighted by the incoherent scattering cross section of their nuclei. Because of the great difference between σ_{inc} of hydrogen and carbon (79.9 b and 0.001 b, respectively) it is sufficient to consider only the hydrogens.

Discrete Fourier transforms were calculated using the fast Cooley-Tukey algorithm, and the transforms were averaged over all chains and normalized to unity over the total energy interval (the frequencies were expressed as $\hbar\omega$ in meV units). The calculated $G(E)$'s for the 173 K simulation are presented in Fig. 8. It is known that the truncation of dynamic data (caused naturally by finite run time) leads to some spectral leakage, resulting in rapidly varying sidelobes around a peak. Therefore the spectrum was smoothed by applying the Blackman window[29] [Fig. 8(a)]. The separation of velocity vectors into components $\mathbf{v}_{\|}$ and $\mathbf{v}_{\perp}$ enables simultaneous evaluation of the density of modes polarized parallel and perpendicular to the c axis [Fig. 8(b)]. The graphs reveal that the rigid-chain simulation reproduces the experimental spectra up to $\sim$ 23 meV; i.e., modes above this energy in the experiment are due to intrachain motion. Furthermore, the simulated $G_{\|}$ is essentially zero beyond 5 meV; in our model, vibrations above this energy are polarized entirely in the perpendicular direction. The calculated maximum in $G(E)$ is near 18 meV, whereas the experimentally determined value is 20 meV. Taking into account such shifting, the measured peak in $G_{\perp}$ below 10 meV could correspond to the well-defined peak (with shoulder) at 6.5 meV [Fig. 8(b)]. Also in the ex-

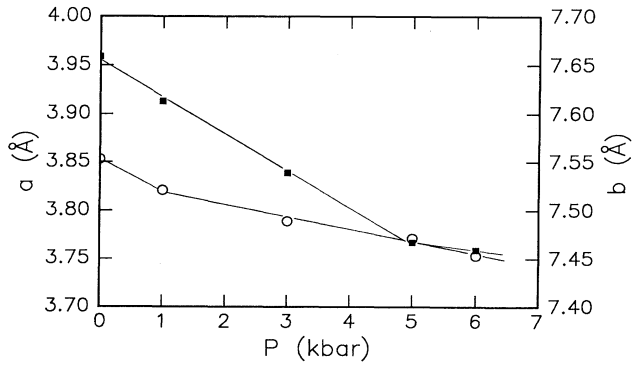

FIG. 6. Pressure dependence of the lattice parameters a (open circles, left scale) and b (solid squares, right scale) from the simulation results.

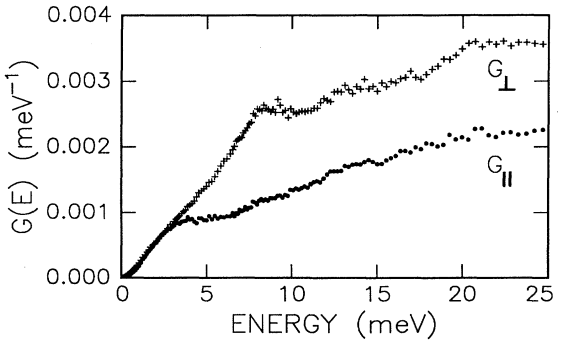

FIG. 7. Polarized vibrational density of states $G(E)$ measured at 295 K on stretch-oriented *trans*-$(CH)_x$ using inelastic incoherent neutron scattering.

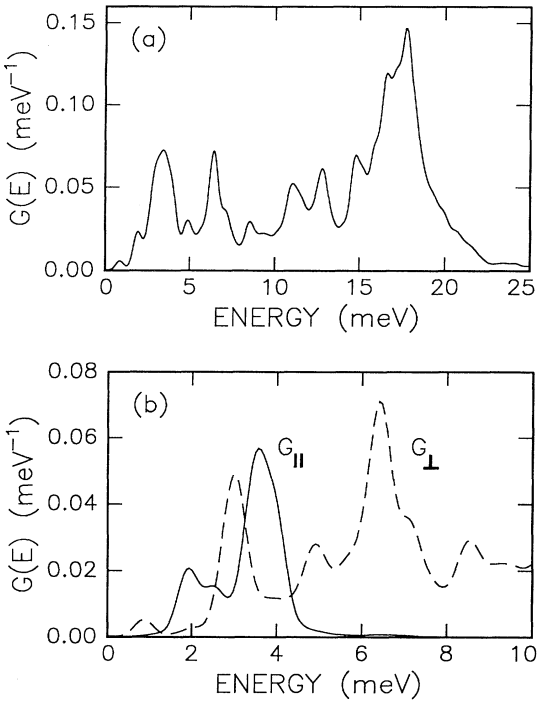

FIG. 8. Smoothed $G(E)$ spectra derived from MD simulations at 173 K: (a) total spectrum; (b) decomposition of (a) into components with hydrogen motions along c ($G_{\|}$, solid curve) and perpendicular to c ($G_{\perp}$, dashed curve).

perimental $G_{\perp}$ there is some structure apparent between 10 and 15 meV, possibly corresponding to the closely spaced peaks at 11, 13, and 15 meV in the simulation results.

Obvious differences between $G_{\|}$ and $G_{\perp}$ are found in both experimental and simulation results. The calculated maximum in $G_{\|}$ at 3.5 meV corresponds very well with the peak (and the following plateau) at this value in the experimental curve. The 3 meV peak in $G_{\perp}$ is not apparent in the data, nor are the lowest frequency peaks at 2 meV ($G_{\|}$) and 0.8 meV ($G_{\perp}$). These discrepancies are possibly due to insufficient experimental resolution and statistics.

Similar spectra were calculated from the simulations at higher temperatures. In these, peak broadening was noticed, especially in the low-frequency region where the peaks of $G_{\|}$ merged together. Also, the amplitude of the 3 meV peak in $G_{\perp}$ decreased relative to the $G_{\|}$ peak, and the weak 0.8 meV peak completely disappeared with increasing T. At high pressure, peaks in the density of states naturally shifted towards higher frequencies. This shift was most remarkable above 10 meV; at 6 kbar the maximum in $G(E)$ shifted from 18 to 21 meV, whereas the $G_{\|}$ peak was only slightly displaced from 3.5 to 4 meV.

Within the rigid-chain approximation, the total motion of H atoms in the lattice is the result of translational and rotational vibrations of the chains. In order to determine the contributions of these vibrations to $G(E)$ we have calculated the Fourier transforms of translational velocity components v_x (in the a direction) and v_y (in the b direction) and of angular velocity of chains. The smoothed power spectra are depicted in Fig. 9. The comparison with Fig. 8 clearly suggests that the main contribution to $G(E)$ comes from chain rotations at higher frequencies and from translations at low frequencies. The presence of 3, 5, 6.5, and 11 meV peaks in all spectra in Fig. 9 further supports the concept of coupling between translational (in the ab plane) and rotational motion. It can also be seen that the weak 0.8 meV peak, present only at low T, originates in the spectrum of angular velocity.

The computed densities of states show richer structure than the experimental spectra. One possible explanation is the small size of the simulated system, since usually small systems exhibit more tendency towards periodic motion, and averages are statistically less representative than in large systems. Another reason can be the intrachain motion not considered in this simulation; if the low-energy intrachain vibrations are chain length dependent, than the polydispersity of the $(CH)_x$ sample would result in the smoothening of $G(E)$. In an independent MD study of short, flexible $(CH)_x$ chains[30] such dependence was in fact observed.

The partial similarity of the experimental $G_{\perp}$ and $G_{\|}$ in the 10–25 meV interval is explained by the experimental technique: The scattered neutrons were detected

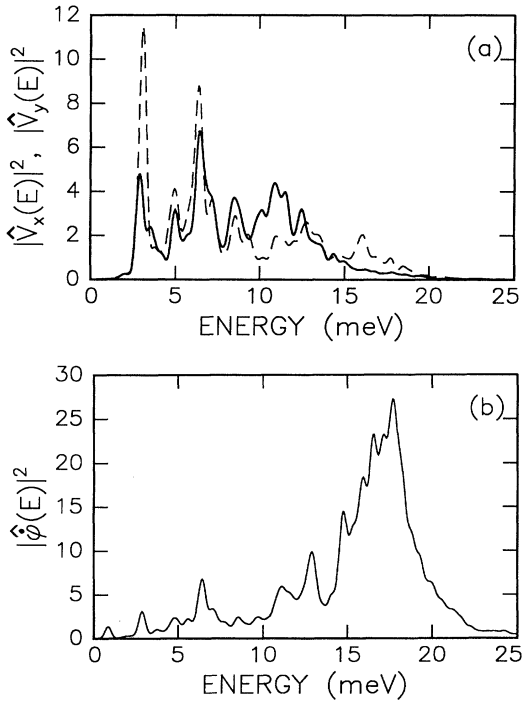

FIG. 9. Velocity power spectra (squared amplitudes of Fourier transforms) at 173 K: (a) translational chain velocity components v_x and v_y (dashed and solid curves respectively); (b) angular velocity of chains. The latter clearly dominates above 15 meV. units are 10^{-3} Å^2 ps^{-2} and 10^{-3} rad^2 ps^{-2}, respectively.

by an array of detectors spanning an angle of more than 20°, and the $(CH)_x$ sample itself had a mosaicity of the c axis of about 30°; therefore complete separation of the two polarizations is not possible and a part of $G_\perp(E)$ is projected to $G_\parallel(E)$ and vice versa.

VI. SUMMARY AND CONCLUSIONS

Constant-pressure simulations of a model lattice of infinite and rigid $(CH)_x$ chains reproduces quite well the anisotropic properties of crystalline *trans*-polyacetylene, the anisotropy in $a(T)$ and $b(T)$ being slightly higher than was observed by x-ray diffraction. Near 417 K an interesting phase transition occurs in the simulated lattice. This consists of simultaneous changes in the orientational order and the onset of liquidlike chain diffusion in the c direction. Analysis of the c-axis motions shows that at 173 K there is no diffusion at all, at 307 K jump diffusion occurs, and above 400 K the jumps are so frequent that the diffusion has more liquidlike character. This phenomenon can be explained as follows. Restoring forces in the c direction are the result of interchain interactions. As T increases, random motions along the c axis increase and the average force field becomes more homogeneous. This reduces the constraints along c, further enhancing the c-axis motion. However, the chains never become truly homogeneous, but the enhanced longitudinal motion changes significantly the dynamics in the ab plane. Whereas at low T (when average c positions of chains are on lattice points) the 2D lattice in the ab plane is formed by two sublattices (chains with setting angles Φ and $-\Phi$), at high T the chain projections in equivalent positions are no longer identical. Thus in a sense the lattice is more quasi-two-dimensional at low T than at higher T. Of course, we might expect that at very high T the chains could be considered as completely homogeneous and the projections have become identical, but probably at such T the melting in the ab plane would also occur. Similar transitions are found in solid n-alkanes just below the melting point, but cannot be probed for in $(CH)_x$ due to the limited thermal stability of the polymer.

The high-P simulations also reproduced quite well the anisotropy in linear compressibilities, while the transition from rectangular to oblique interchain packing symmetry did not appear in the calculation. The sensitivity of the method in the determination of γ was certainly sufficient to detect this effect, since in the $P = 0$ simulations the average value of γ remained very close to 90° in spite of the shearing of the simulation box during the runs.

Polarized vibrational densities of states are in very good agreement with the low-frequency part of the spectra obtained by inelastic incoherent neutron scattering. Even though no artificial constraints for the motion in the c direction were introduced, the 3.5 meV peak in the parallel polarization was reproduced in excellent agreement with the experiment. Rigid-chain motion contributes to $G(E)$ for energies up to 23 meV, with the maximum originating in chain rotations. By comparing the experimental graphs with the simulation results, distinct features in the data can be assigned with confidence: 3.5 meV peak in $G_\parallel$ to rigid-body vibrations along the chain axis, ~ 8 meV to whole-body chain vibrations in the ab plane, and ~ 20 meV in $G_\perp$ to chain librations.

Discrepancies in absolute values between simulated and experimental results can be attributed in part to the small size of the simulation box, but mainly to limitations in the model potential. The simulated lattice is more tightly packed in the a direction than the real one, leading naturally to smaller setting angle and larger b parameter. This is also reflected by the observation that the model lattice stiffens in the a direction with increasing P already at 1 kbar. The (exp –6) potential function, with the same parameters A, B, C as we used, worked very well in simulations of polyethylene and n-alkanes. However, as was already noted by Williams,[22] this site-site potential was fitted to crystalline nonaromatic hydrocarbons and aromatic hydrocarbons in which π-electron interactions did not introduce any large effects. This might not be the case in polyacetylene where the double bonds could play an important role in the character of interchain interactions. A simple remedy to the model potential would be to place a small negative partial charge in the centers of double bonds (or on carbon sites) and positive partial charges in H sites. The increased repulsion between H sites should result in increasing Φ and the repulsion between C sites could also increase the a distance. A similar strategy is necessary to reproduce the ordered structure of solid C_{60}.[31]

We have demonstrated that MD simulations performed on a very simple model of crystalline *trans*-$(CH)_x$ can provide useful information on this molecular crystal. An obvious extension is the study of doped structures, with special attention to the problem of how the interchain dynamics contribute to the electronic properties of these materials.

ACKNOWLEDGMENTS

We thank J. L. Sauvajol for supplying the neutron-scattering results for *trans*-$(CH)_x$. Helpful discussions with Ailan Cheng and M. L. Klein are also gratefully acknowledged. This work was supported by the National Science Foundation MRL Program under Grant No. DMR91-20668.

[1] H. Shirakawa and S. Ikeda, Polym. J. **2**, 231 (1971).
[2] H. Shirakawa, T. Ito, and S. Ikeda, Polym. J. **4**, 460 (1973).
[3] C. K. Chiang, Y. W. Park, A. J. Heeger, H. Shirakawa, E. J. Louis, and A. G. MacDiarmid, J. Chem. Phys. **69**, 5098 (1978).
[4] W. P. Su, J. R. Schrieffer, and A. J. Heeger, Phys. Rev. Lett. **42**, 1698 (1979).
[5] H. Naarmann and N. Theophilou, Synth. Met. **22**, 1 (1987).

[6] K. Akagi, M. Suezaki, H. Shirakawa, H. Kyotani, K. Shimamura, and Y. Tanabe, Synth. Met. **28**, D1 (1989).
[7] Y. Cao, P. Smith, and A. J. Heeger, Polymer **32**, 1210 (1991).
[8] J. C. W. Chien, F. E. Karasz, and K. Shimamura, Macromolecules **15**, 1012 (1982).
[9] C. R. Fincher, C. E. Chen, A. J. Heeger, A. G. MacDiarmid, and J. B. Hastings, Phys. Rev. Lett. **48**, 100 (1982).
[10] H. Kahlert, O. Leitner, and G. Leising, Synth. Met. **17**, 467 (1987).
[11] Q. Zhu, J. E. Fischer, R. Zuzok, and S. Roth, Solid State Commun. **83**, 179 (1992).
[12] P. A. Heiney, J. E. Fischer, D. Djurado, J. Ma, D. Chen, M. J. Winokur, N. Coustel, P. Bernier, and F. E. Karasz, Phys. Rev. B **44**, 2507 (1991).
[13] H. A. Mizes and E. M. Conwell, Phys. Rev. Lett. **70**, 1505 (1993).
[14] M. R. Anderson, K. Väkiparta, M. Reghu, Y. Cao, and D. Moses, Phys. Rev. B **47**, 9238 (1993).
[15] J. Ma, J. E. Fischer, E. M. Scherr, A. G. MacDiarmid, M. E. Józefowicz, A. J. Epstein, C. Mathis, B. Francois, N. Coustel, and P. Bernier, Phys. Rev. B **44**, 11609 (1991).
[16] J. Ma, J. E. Fischer, Y. Cao, and A. J. Heeger, Solid State Commun. **83**, 395 (1992).
[17] P. R. Swan, J. Polym. Sci. **56**, 403 (1962).
[18] G. T. Davis, P. K. Eby, and J. P. Colson, J. Appl. Phys. **41**, 4316 (1970).
[19] J. L. Sauvajol, D. Djurado, A. J. Dianoux, N. Theophilou, and J. E. Fischer, Phys. Rev. B **43**, 14305 (1991).
[20] J.-P. Ryckaert and M. L. Klein, J. Chem. Phys. **85**, 1613 (1986).
[21] J. T. Lopez Navarette and G. Zerbi, Solid State Commun. **64**, 1183 (1987).
[22] D. E. Williams, J. Chem. Phys. **47**, 4680 (1967).
[23] H. C. Andersen, J. Chem. Phys. **72**, 2384 (1980).
[24] M. Parrinello and A. Rahman, Phys. Rev. Lett. **45**, 1196 (1980).
[25] S. Nosé and M. L. Klein, Mol. Phys. **50**, 1055 (1983).
[26] C. F. Gerald and P. O. Wheatley, *Applied Numerical Analysis* (Addison-Wesley, Reading, MA, 1970), p. 320.
[27] M. P. Allen, D. J. Tildesley, *Computer Simulation of Liquids* (Clarendon Press, Oxford, 1990), p. 82.
[28] M. G. Broadhurst, J. Res. Natl. Bur. Stand. A **66**, 241 (1962).
[29] F. J. Harris, Proc. IEEE **66**, 51 (1978).
[30] A. J. Dianoux, G. R. Kneller, J. L. Sauvajol, and J. C. Smith, J. Chem. Phys. (to be published).
[31] M. Sprik, A. Cheng, and M. L. Klein, J. Phys. Chem. **96**, 2027 (1992).